Tunable and compact permanent magnet uniform spreading beamline for electron irradiation accelerators

Zijian Zhou, Keyan Sheng, Zhenyi Zhang, Mianzhi Xiong, Haozhe Li, and Jiang Huang*

State Key Laboratory of Advanced Electromagnetic Technology (Huazhong University of Science and Technology), Wuhan 430074, China

(Received 24 May 2023; accepted 5 September 2023; published 29 September 2023)

The growing interest in the field of electron irradiation accelerators has led to various research opportunities, with a crucial emphasis on enhancing the irradiation homogeneity of accelerators to advance the industry of the irradiation process. In this study, we introduce a tunable and compact uniform spreading beamline that comprises a permanent magnet quadrupole doublet and an electron beam permanent magnet spreading system. This beamline could solve the problem of poor irradiation homogeneity caused by irregular beam spots in electron irradiation accelerators. Flexible and tunable magnetic yokes enable rapid changes to the magnetic field distribution based on different beam spot profiles or irradiation processing requirements, achieving uniform spreading of different beam spots and improving irradiation homogeneity. Additionally, we evaluated the performance of rectangular permanent magnet poles to minimize errors in future accelerator applications. The implementation of this beamline enhances irradiation quality and provides an experimental foundation for further investigating the interaction between electron beam irradiation rates and materials.

DOI: 10.1103/PhysRevAccelBeams.26.092402

I. INTRODUCTION

Energetic electron beam irradiation is a unique method that utilizes the physical, chemical, and biological effects generated by the high-velocity electrons interacting with substances to modify their properties and achieve desired characteristics [1–4]. In essence, electron irradiation employs a physical approach to address chemical problems. Due to their rapid irradiation speed, enhanced efficiency, safety, and reliability [5–7], electron irradiation accelerators have increasingly replaced traditional ^{60}Co sources as the primary device for irradiation processing applications such as sterilization, wastewater treatment, and breeding [8–10]. Irradiation homogeneity is a crucial parameter in ensuring consistent product quality and feasibility of techniques in these applications. Additionally, precise control of the electron beam is essential for investigating the interaction mechanism between the beam and materials when developing high-performance materials through electron beam irradiation [11–14].

In recent years, the utilization of multipole magnets for achieving beam homogenization has garnered increasing attention. The concept of employing an octupole magnet for beam homogenization was initially proposed by Meads [15]. Kashy and Sherrill subsequently validated the homogenization effect of octupole magnets through numerical calculations conducted on a specific optical path [16]. Furthermore, they demonstrated that an odd-order multipole magnetic field is essential for achieving beam homogenization with a Gaussian distribution [17]. Blind employed numerical methods to investigate the issues pertaining to beam sizing and beam jitter in large beams [18]. Meot and Aniel derived the required magnetic field strength for a specific optical path [19], while Yuri *et al.* theoretically determined both the necessary magnetic field strength and the beam size for an odd-order multipole magnetic field configuration [20]. However, limited research has been conducted thus far regarding the application of multipole magnets in electron irradiation accelerators. The conventional transport of the electron beam from the accelerating tube to the target could be considered a short beamline composed of a focusing system and a scanning system [21,22] utilizing solenoids and scanning magnets, respectively. Extensive studies have been conducted on principles such as solenoids' impact on focusing beams, triangular current waveforms' or triangular and sinusoidal synthetic waveforms' impact on achieving homogeneous radiation and improving irradiation homogeneity [21,23,24].

*Corresponding author: jhuang@hust.edu.cn

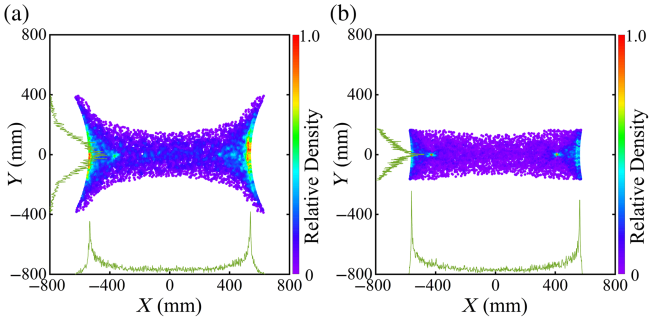

FIG. 1. Spreading results of irregular beam spot: (a) large circular and (b) elliptical.

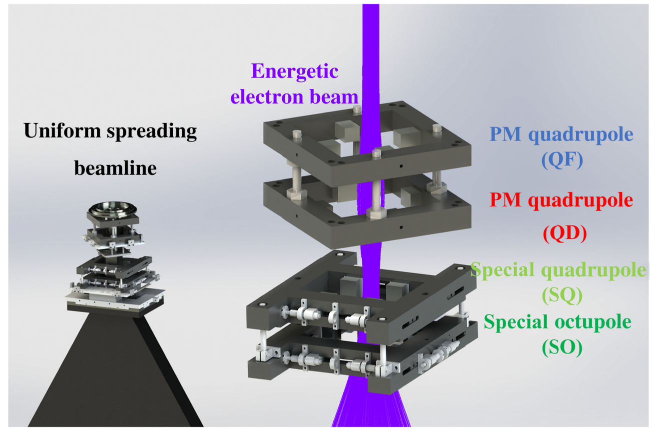

FIG. 2. The tunable and compact uniform spreading beamline for electron irradiation accelerators.

However, scanning magnets often present significant challenges such as tail sweep [25], high power consumption, and heat generation, resulting in poor irradiation homogeneity (excessive doses at both ends) and energy loss, which necessitate frequent maintenance and repair [26]. We have previously reported on replacing the scanning magnet with a permanent magnet (PM) electron beam spreading system in a 0.5 MeV electron irradiation accelerator, where some of these issues were largely solved by constructing a special octupole magnetic field for achieving uniform electron spreading [26,27]. As we extend this application from low-energy accelerators to medium-energy accelerators, the PM spreading system encounters additional challenges and problems, particularly irregular beam spots [28]. For instance, solenoids with weak focusing ability are unable to correct irregular beam spots effectively, leading to highly disordered electron distribution that may even exceed the size of the scanning box (typically horizontal size <1200 mm and vertical size <100 mm), as shown in Fig. 1. Under such conditions, a large number of electrons will impact the scanning box, resulting in significant heat generation that can damage the vacuum environment or even cause shutdowns within the accelerator facility. Given these challenges posed by irregular beam spots along with requirements for irradiation production and scientific research in electron irradiation accelerators, it is imperative to construct a new beamline using novel methods that offer high homogeneity and flexible tunability.

For the requirement of a special rectangular uniform beam target, the paper proposes a uniform spreading beamline to achieve electron beam homogenization for a 3-MeV electron irradiation accelerator. The beamline consists of a PM spreading system and a permanent magnet quadrupole (PMQ) doublet, as illustrated in Fig. 2. The compact design of the beamline is achieved by utilizing PMs as magnetic poles. To establish the basis for subsequent beam regulation (Sec. II), we investigate the effects of magnetic pole layout on the special magnetic field. In order to provide a detailed description of the transport process on this beamline, we employ uniform beam spreading of a circular beam spot as an example. Through beam simulation results, it is demonstrated that adjusting the magnetic parameters using four sets of magnets can achieve uniform beam spreading for both circular and elliptical beam spots (Sec. III). Furthermore, we design and optimize the magnetic yoke to ensure flexible adjustment of the magnetic field under different conditions. Additionally, we measure and screen the performance of PMs to ensure consistency between practical measurements and numerical simulation results regarding their magnetic fields, thereby reducing potential application errors (Sec. IV).

II. MAGNET DESIGN

Typically, in an electron irradiation accelerator, the total length between the focusing solenoid and magnet scanning systems does not exceed 0.5 m. Due to its compact space requirements and energetic electrons with high magnetic rigidity, rubidium-iron-boron (Nd-Fe-B) PMs are considered an optimal choice for serving as multipole magnets' magnetic poles. Unlike electromagnets, the magnetic field of PMs can only be regulated by adjusting their structures and layouts. The detailed magnet design is shown below.

A. Permanent magnet spreading system

Previous studies on multipole magnets [15–19,29,30] have shown that the optimum nonlinear magnetic field strength required for beam homogenization, and the full width of the target region could be expressed as below:

$$K_{2n} = \frac{(-1)^{\frac{n}{2}}(n-2)!}{(\frac{n}{2}-1)!(2\varepsilon\beta_0)^{\frac{n}{2}-1}\beta_0\,\tan\varphi}\quad(n=4,6,8,\ldots), \tag{1}$$

$$K_{2n-1} = 0, \tag{2}$$

$$2r_t = \sqrt{2\pi\varepsilon\beta_t}|\cos\varphi|. \tag{3}$$

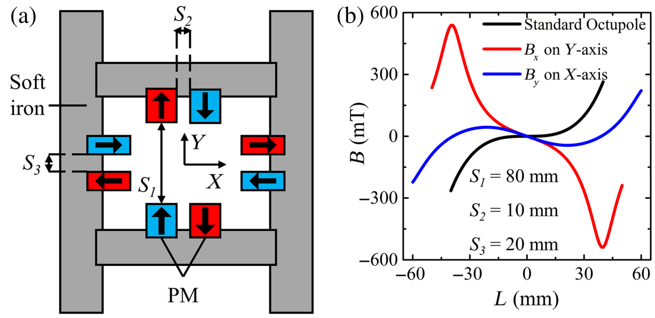

FIG. 3. (a) Special octupole magnet and (b) comparison with a standard octupole magnetic field strength with the same aperture (80 mm).

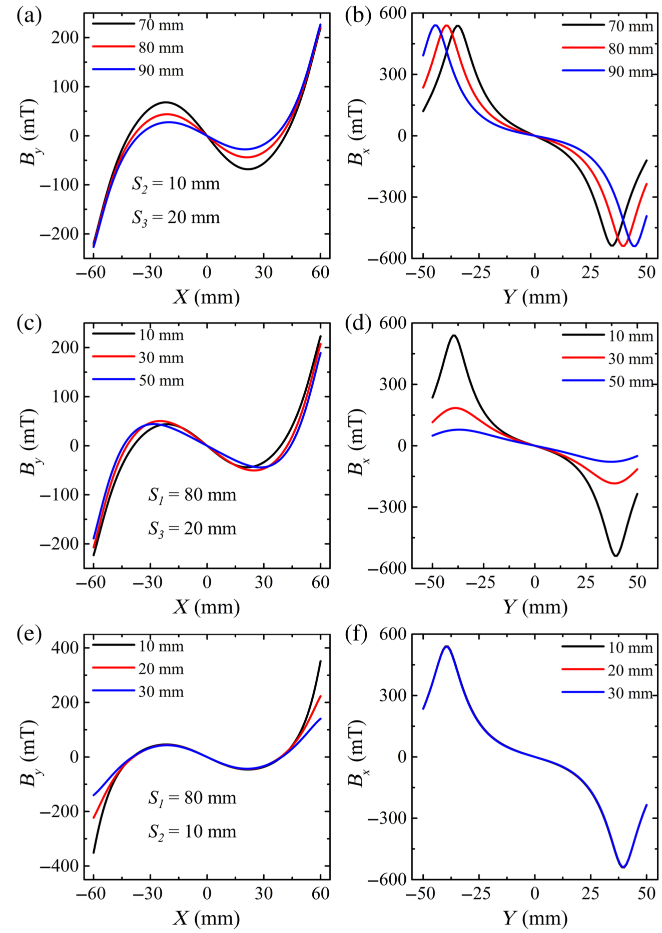

FIG. 4. Variation in (a) B_y and (b) B_x as a function of S_1 under $S_2 = 10$ mm and $S_3 = 20$ mm; variation in (c) B_y and (d) B_x as a function of S_2 under $S_1 = 80$ mm and $S_3 = 20$ mm; variation in (e) B_y and (f) B_x as a function of S_3 under $S_1 = 80$ mm and $S_3 = 10$ mm.

Where, K_{2n} and K_{2n-1} are magnetic fields strength, ε is the emittance of the initial beam spot, φ is the phase advance, and r_t is the half-width of the target region. According to Eqs. (1) and (2), odd-order nonlinear magnetic fields K_{2n} ($n = 4, 6, 8, \cdots$), particularly the octupole magnetic field, are necessary for beam homogenization. However, standard octupole magnets have limitations in electron irradiation accelerators due to their lack of significant beam spreading effect and centrally rotationally symmetrical magnetic field structure [20,31]. These two problems lead to an approximate small square beam distribution in the target region, which is not suitable for electron irradiation accelerators that require rectangular irradiation fields.

Drawing on previous research, coupling a linear magnetic field (quadrupole magnetic field) into an octupole magnetic field might be a solution to achieve horizontal beam homogenization and obtain a large horizontal beam width at the same time. By changing the layout of the standard octupole magnet, a special octupole magnet (SO) is obtained. The detailed structure and specific magnetic parameters of the SO compared to a standard octupole with the same aperture are shown in Fig. 3 and Table I, respectively.

As depicted in Fig. 3(b), in the horizontal direction, the magnetic field B_y within the paraxial-axis region exhibits an approximate quadrupole magnetic field, which could change the β of the beam and ultimately lead to an increase in horizontal target width. While the off-axis region exhibits an approximate octupole magnetic field B_y, which is utilized for beam homogenization in the horizontal direction. There is an extreme point between the quadrupole magnetic field and the octupole magnetic field at the position of $x = \pm 21$ mm. The critical point of this special magnetic field is referred to as the magnetic demarcation point, playing a crucial role in subsequent beam regulation. Figure 4 illustrates the variations in the SO's magnetic field resulting from adjustments made to its magnetic parameters S_1, S_2, and S_3.

When solely relying on a single SO for beam homogenization, electron spreading could be challenging due to the weak strength of the octupole magnetic field. To achieve the desired beam homogenization effect, it would be necessary to increase the remanence of permanent magnets up to 5.0 T; however, this exceeds manufacturing capabilities for Nd-Fe-B PMs. In order to reduce reliance on high remanence value, according to the octupole magnetic field expression $K_8 = 1/(2\varepsilon\beta_0{}^2 \tan\varphi)$, increasing the β will lead to a reduction in octupole magnet

TABLE I. Magnetic parameters of spreading system.

Parameters	SO	SQ
Size of PMs (mm^3)	$30 \times 30 \times 35$[a] $20 \times 30 \times 45$[b]	$30 \times 30 \times 35$
Br of PMs (T)	1.3	1.3
Insert depth (mm)	15	15
Grade of PMs	N42H	N42H
Length in Z (mm)	40	40

[a]Size for four big magnets in SO.
[b]Size for four small magnets in SO.

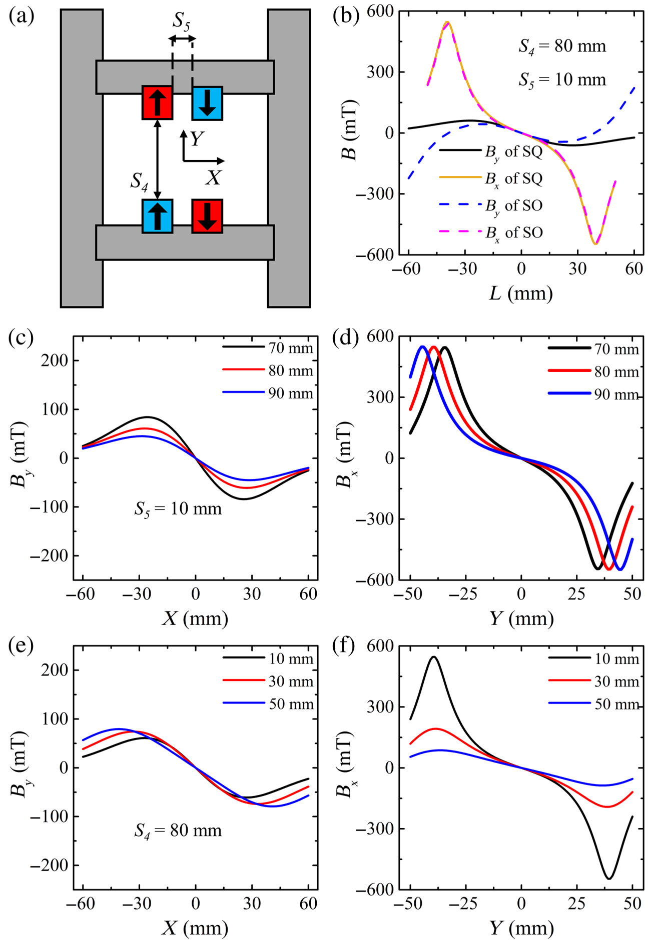

FIG. 5. (a) Special quadrupole magnet and (b) comparison with special octupole magnet; variation in (c) B_y and (d) B_x as a function of S_4 under $S_5 = 10$ mm; variation in (e) B_y and (f) B_x as a function of S_5 under $S_4 = 80$ mm.

strength. Therefore, a special quadrupole magnet (SQ) is introduced before SO as depicted in Fig. 5(a), with a comparison of SQ and SO's respective magnetic field strengths shown in Fig. 5(b). Table I also provides details regarding these specific magnet parameters. By ignoring X', new horizontal direction β and K_8 are as follows:

$$X_t = X_0 \cos h(K_4 L), \tag{4}$$

$$\beta_t = \frac{X_t{}^2}{\varepsilon} > \frac{X_0{}^2}{\varepsilon}, \tag{5}$$

$$K_8 = 1/(2\varepsilon\beta_t{}^2 \tan\varphi) < 1/(2\varepsilon\beta_0{}^2 \tan\varphi). \tag{6}$$

From Eq. (6), the magnetic field strength K_8 of the octupole magnet could be reduced. By combining these two special magnets together, beam homogenization is successfully achieved by using PMs with only 1.3 T remanence requirements. Similarly, Figs. 5(c) through 5(f) demonstrate changes in SQ's magnetic field resulting from alterations made to its magnetic parameters S_4 and S_5.

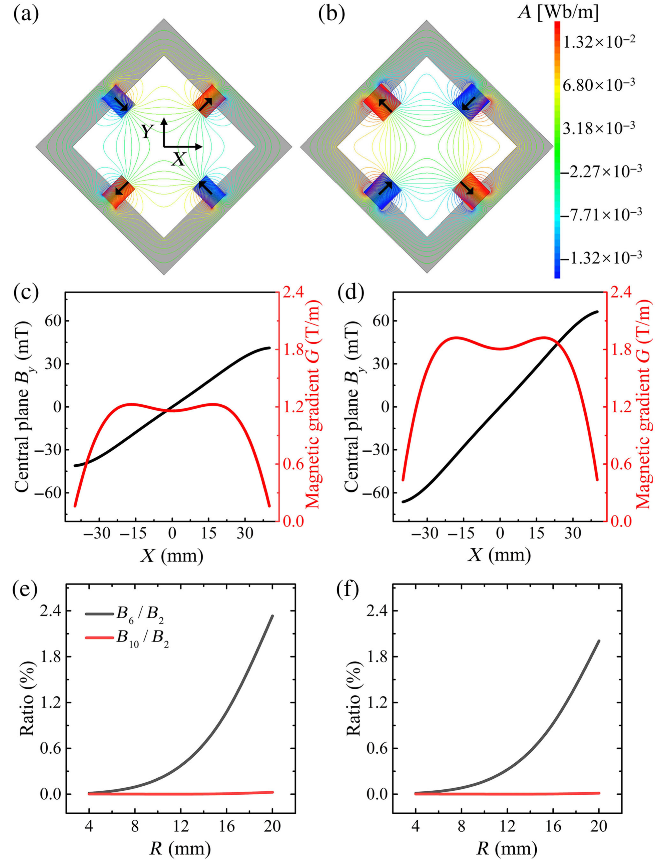

FIG. 6. (a) PMQ-QF; (b) PMQ-QD; center plane magnetic field strength and magnetic field gradient of (c) QF and (d) QD; analysis of the harmonic components of (e) QF and (f) QD.

B. Permanent magnet quadrupole doublet

As depicted in Figs. 6(a) and 6(b), the PMQ doublet comprises two sets of PMQs with alternating magnetic field gradients. This design is based on a simplified Halbach PMQ structure [32–39], which consists of only four PMs and DT4 yokes. The first set is referred to as QF, while the second set is called QD. As shown in Figs. 6(c) and 6(d), both PMQs exhibit good linearity between their paraxial magnetic field B_y and X-axis, with little high-order multipole components except for quadrupoles as demonstrated by Figs. 6(e) and 6(f). Table II provides detailed information about the magnetic parameters of these two PMQs.

The regulation of electron beams by this doublet involves adjusting coupling magnetic fields through varying center distances between these two sets of magnets due to their small mechanical length along beam transport direction (as illustrated in Fig. 7). Magnetic field integral GL significantly depends on distance variations, which greatly affects focusing ability of this doublet and further influences beam spreading effect within beamline.

TABLE II. Magnetic parameters of doublet.

Parameters	QF	QD
Size of PMs (mm^3)	22 × 22.5 × 32	22 × 30 × 33
Br of PMs (T)	1.3	1.3
Insert depth (mm)	15	15
Aperture (mm)	58	57
Grade of PMs	N42H	N42H
Length in Z (mm)	32	35
G (T/m)	1.156	1.801
Good field (mm)	40	40
Homogeneity	94.62%	93.78%

III. BEAM DYNAMICS SIMULATION

One of the drawbacks of using PMs in particle accelerators is their fixed magnetic field. Here we demonstrate a new method to showcase the tunability of our PM system under different conditions. By utilizing the unique beam regulation ability of each magnet, we replaced the traditional solenoid focusing system with a PMQ doublet and used a PM spreading system instead of a scanning magnet in our uniform spreading beamline design. As shown in Fig. 8, the magnet arrangement on the beamline is QF-QD-SQ-SO, where D_1 represents the center distance between QF and QD, D_2 represents the center distance between QD and SQ, and D_3 represents the center distance between SQ and SO. After passing through SO, the beam reaches its final target via a free drift distance of 1.2 m spreading box (original scanning box).

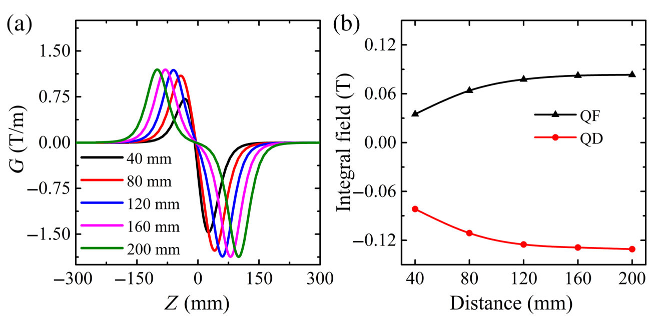

FIG. 7. (a) Variation in coupling magnetic field on the Z axis and (b) integral field GL as a function of center distance of the doublet.

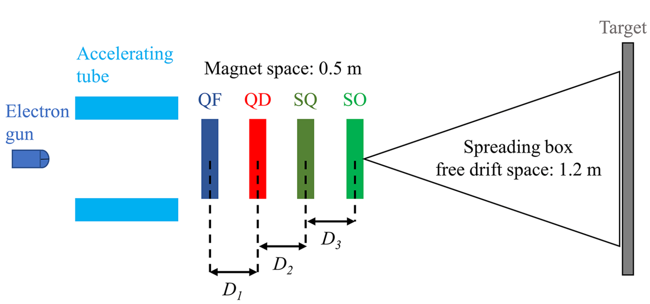

FIG. 8. Simplified model of uniform spreading beamline.

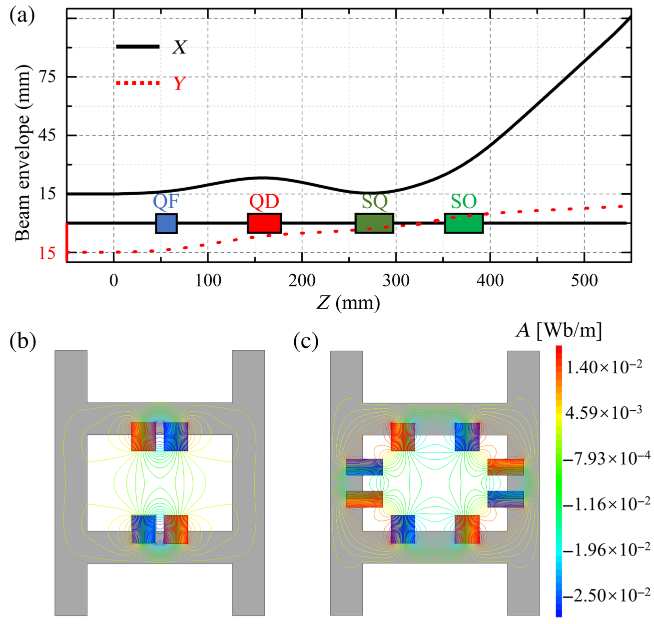

FIG. 9. (a) Beam envelope of the beamline, magnetic field of (b) SQ, and (c) SO.

A. Large circular Gaussian beam spots

Circular Gaussian beam spots are commonly produced by electron guns in electron irradiation accelerators [40]. Therefore, achieving uniform spreading of circular beam spots is fundamental for any beam transport line. Figure 9 illustrates significant parts of uniform spreading beam envelope for circular beams as well as SQ and SO magnetic fields under such conditions; specific parameters for this particular setup are presented in Table III. Given that circular beams are frequently used in irradiation processing applications, these adjustment parameters hold considerable significance.

Due to the space charge effect and electric repulsion, the electrons produced by the Pierce electron gun will diverge in space, resulting in the nearly same divergence in both phase spaces (X, X') and (Y, Y'). In this dynamic simulation, the

TABLE III. Fundamental beamline parameters.

Parameters	Value (mm)
S_1	80
S_2	25
S_3	20
S_4	80
S_5	10
D_1	98.5
D_2	117.5
D_3	95

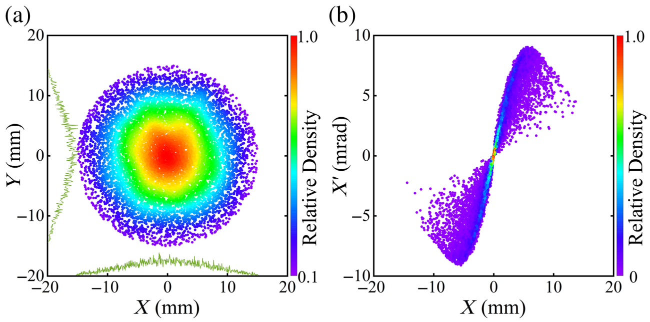

FIG. 10. The (a) profile and (b) the (X, X') phase space of the initial large round Gaussian beam spot.

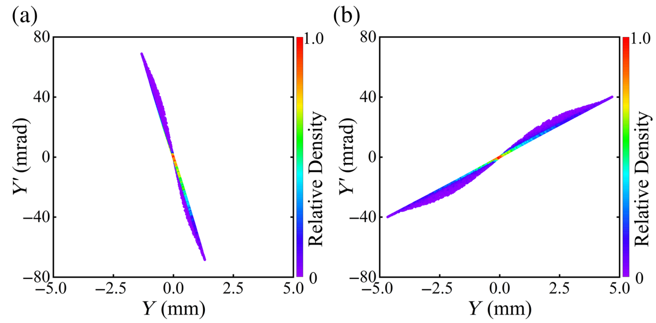

FIG. 12. The vertical phase space of electrons at the position of (a) leaving the SO ($Z = 297$ mm) and (b) leaving the SO ($Z = 392$ mm).

initial beam spot after the accelerating tube has a radius of 15 mm and an energy of 3 MeV as illustrated in Fig. 10. The emittance of the beam spot is sufficiently small to be considered approximately parallel to the direction of beam transport.

Upon entering the beam transport line, the beam spot is initially focused by the PMQ doublet, which allows for simultaneous focusing in both directions due to its strong focusing with alternating gradients. After passing through the doublet, the beam spot travels through a free drift space between the QD and SQ. As shown in Fig. 11, the focused beam spot that enters into the SQ spreading system is an ever-shrinking ellipse.

Due to the unique structure, standard linear transport matrices cannot be used to calculate trajectories for SQ and SO in spreading systems; therefore, separate analyses are conducted on horizontal and vertical directions' envelope beams to illustrate their respective transport principles. For electrons of beam envelope in the vertical direction, experiencing a focusing force in SQ, which results in electrons crossing the quadrant in the free drifting space between SQ and SO. In SO, electrons experience the same focusing force once again. The transport process is similar to that of a quadrupole magnet doublet with two same magnetic field gradients. As illustrated in Fig. 12, the electron's vertical phase undergoes reversal upon passing through the spreading system, leading to a significantly

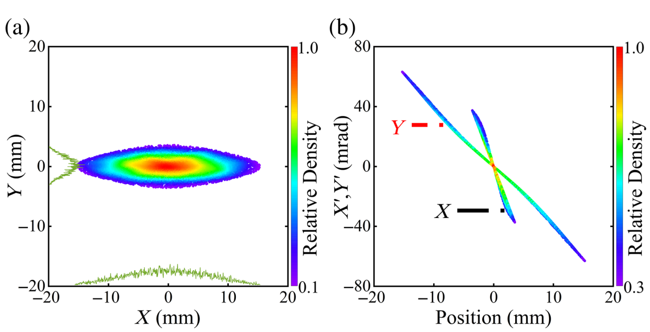

FIG. 11. The (a) profile and (b) phase space of the beam spot about to enter the spreading system.

reduced vertical envelope compared with subsequent horizontal motion; thus decoupling the amplitude of vertical motion from horizontal motion [20].

In the horizontal direction, electrons with a small profile will first experience a defocusing force (opposite to their initial velocity) that is produced by a linear quadrupole magnetic field in the SQ, which increases their horizontal β to effectively use subsequent nonlinear magnetic fields [20]. Upon entering the SO, electron trajectories could be divided into two stages depending on whether they reach the magnetic demarcation point. During the first stage of SO, due to the small profile of the horizontal beam envelope, electrons are still subject to action by paraxial-axis linear quadrupole magnetic fields that further increase their horizontal β until reaching the magnetic demarcation point. The off-axis odd-order nonlinear octupole field then causes a fold at the tail end of phase space for external electrons while inner electrons remain outwardly spread for they are still in the linear quadrupole magnetic field as shown in Fig. 13(c). This stage will continue until the electrons reach the free drift space to make high-density internal electrons constantly spread outward through the quadrupole magnetic field, while the external electrons are restricted by the octupole magnetic field. In addition, electrons at oblique angles experience a Lorentz force that pulls them obliquely outward and modifies electron distribution in edge regions. Through comprehensive regulation by four magnets, electron distribution on the target becomes approximately uniform rectangular with a large horizontal beam envelope after passing through free drift space.

Figure 14 shows the target electron distribution results and the numbers of electrons in each area for large circular Gaussian beam spots. The homogeneity of the target is calculated by Eq. (7), which is 91.54% and better than the traditional method of scanning and fully satisfies irradiation production requirements [41,42].

$$\text{Irradiation homogeneity} = \left(1 - \frac{N_{\max} - N_{\min}}{N_{\max} + N_{\min}}\right) \times 100\%. \tag{7}$$

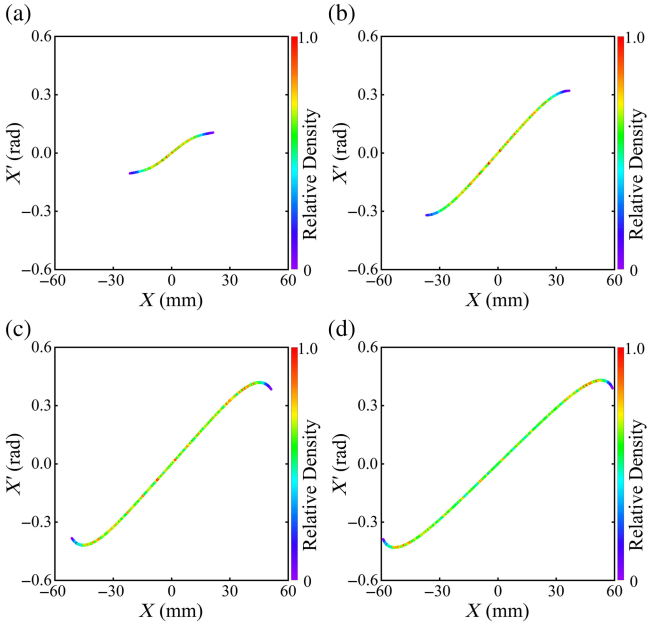

FIG. 13. The horizontal phase space of electrons at the position of (a) leaving the SQ ($Z = 297$ mm), (b) reaching the magnetic demarcation point ($Z = 372$ mm), (c) leaving the SO ($Z = 392$ mm), and (d) leaving the SO by 20 mm ($Z = 412$ mm).

In the smaller range of the target, such as 75% or 50%, the irradiation homogeneity is even close to 95% as shown in Fig. 14(c), which is highly advantageous for irradiating small objects that require a high level of irradiation homogeneity. Any type of electron beam spot entering

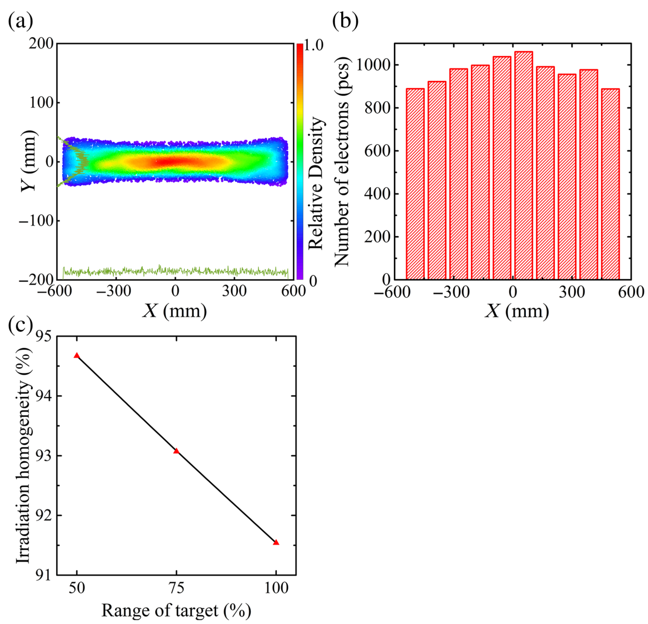

FIG. 14. (a) The target electron distribution; (b) electrons statistics in each irradiation area; and (c) irradiation homogeneity at different ranges of the target.

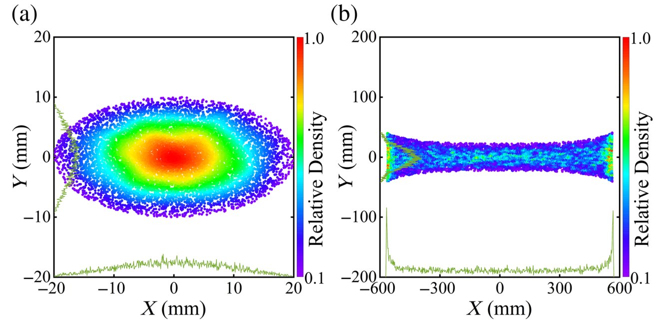

FIG. 15. (a) Elliptical beam spots with a major axis on the X axis and (b) the target electron distribution.

the doublet and spreading system will exhibit a trend similar to the above beam transport. The difference is that the detailed trend may vary depending on the arrangement of magnets and the profile of different beam spots.

B. Horizontal elliptical beam spots

The electron distribution of the elliptical beam spot (with the major axis on the X axis) is depicted in Fig. 15, obtained through direct transport using the uniform spreading beamline without any change made to the aforementioned fundamental parameters.

The electron distribution of the horizontal elliptical beam spot exhibits excessive density at both ends. In comparison to the circular beam spot, the horizontal beam spot displays a greater overall horizontal position upon entering the SQ after passing through the same doublet. Consequently, this results in a heightened Lorentz force acting on the electrons within the SQ and an increased horizontal β. The original spacing between the SQ and SO, which was initially suitable, causes electrons to disperse outwardly more extensively and reach the magnetic demarcation point in advance. As a result, they become overly confined by the octupole magnetic field in the SO, leading to an accumulation of electrons at both ends.

To address this problem, we have increased the distance S_5 of the SQ in order to reduce linear magnetic field strength and Lorentz force. Additionally, we have decreased the distance D_3 between SQ and SO to minimize drift space for horizontally spreading electrons. The revised parameters for our new beamline are presented in Table IV. Figure 16 illustrates that these adjustments have resulted in

TABLE IV. New beamline parameters for horizontal elliptical beam spot.

Parameters	Value
S_5 (mm)	35
D_3 (mm)	69
Homogeneity in 100% target area (%)	92.58
Homogeneity in 75% target area (%)	95.77
Homogeneity in 50% target area (%)	94.66

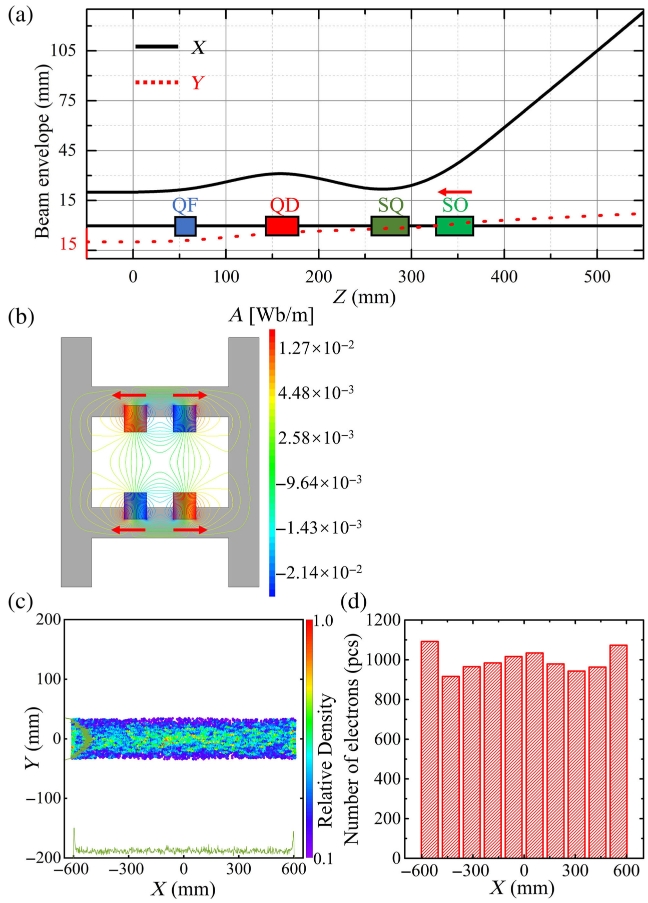

FIG. 16. (a) New beam envelope, (b) new magnetic field distribution of the SQ after adjustment, (c) the target electron distribution, and (d) electrons statistics in each irradiation area of horizontal elliptical beam spots.

improved beam envelope characteristics as well as a more uniform spread of horizontal elliptical beam spots. As a result of these modifications, there has been a significant enhancement in irradiation homogeneity from 61.55% to 92.58%.

C. Vertical elliptical beam spots

Another common type of elliptical beam spot is one with its major axis aligned with the Y axis. By maintaining the fundamental parameters and passing the vertical elliptical beam through the same beamline, its target electron distribution could be obtained as shown in Fig. 17.

The resulting target beam distribution remains Gaussian, exhibiting high density around the origin and low density at both ends in the horizontal direction, while achieving a poor irradiation homogeneity of 56.89%. This is due to a small horizontal envelope of the vertical elliptical beam spot where electrons reach the magnetic demarcation point later than the above two other spots under identical magnetic parameters, leading to inadequate folding of phase by octupole magnetic field in SO and poor

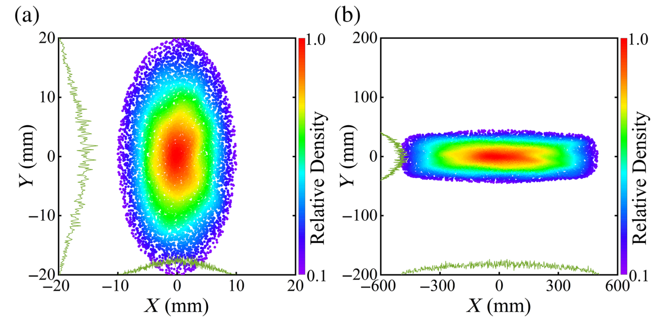

FIG. 17. (a) Elliptical beam spots with a major axis on the Y axis and (b) the target electron distribution.

homogenization effect. To address this issue, several adjustments are made including reducing the distance D_2 to decrease drift space after doublet and increase horizontal envelope before entering the spreading system; increasing distance D_3 for increased drift space for horizontal electron spreading and reaching magnetic demarcation point earlier; reducing distances S_5 and S_2 to enhance linear magnetic field strength throughout spreading system; further decreasing distance S5 to increase the position of demarcation point. All adjusted beamline parameters are specifically listed in Table V while new beam envelope and magnet layouts are illustrated in Figs. 18(a) to 18(c). By adjusting the magnetic field distribution of SQ and SO as well as magnet arrangement across the entire system, the target distribution shape slightly deviates from ideal but irradiation homogeneity improves significantly up to 91.57%.

D. Beam regulation of doublet

In addition to adjusting the distance between the SQ of the spreading system and QD of the doublet, the magnetic field center distance D_1 of QF and QD is also a significant parameter for controlling the beamline, as it can greatly influence the shape and phase space of the beam spot prior to entering the spreading system. Taking a circular Gaussian beam spot as an example, three different spreading results are obtained in Fig. 19 by solely varying the D_1 while keeping other parameters constant. With an equal number of particles, this leads to variations in the target

TABLE V. New beamline parameters for vertical elliptical beam spot.

Parameters	Value
S_2 (mm)	44
S_3 (mm)	15
S_5 (mm)	5
D_2 (mm)	87.5
D_3 (mm)	100
Homogeneity in 100% target area (%)	91.57%
Homogeneity in 75% target area (%)	94.32%
Homogeneity in 50% target area (%)	93.11%

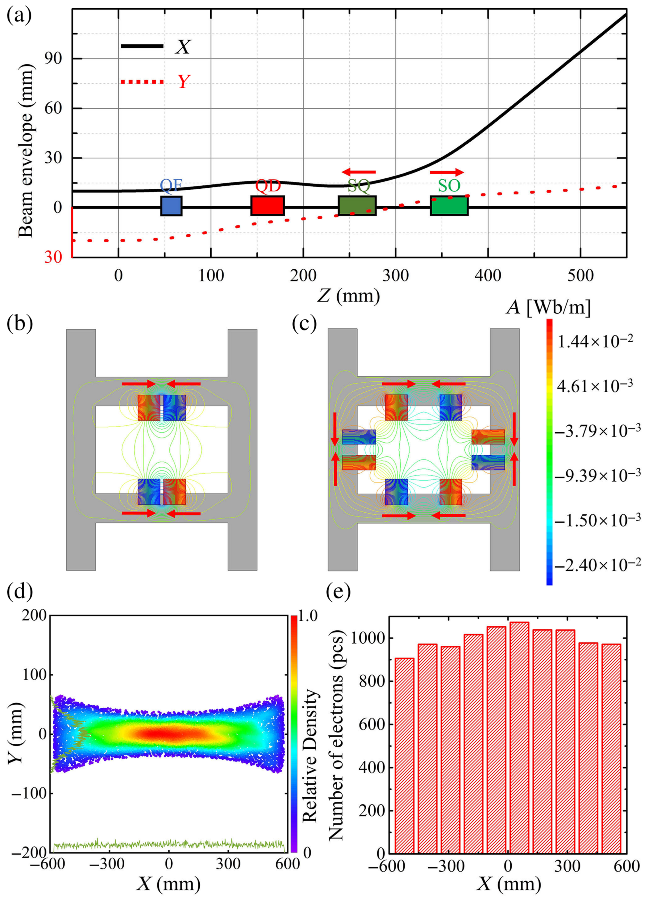

FIG. 18. (a) New beam envelope, magnetic field distribution of (b) SQ and (c) SO after adjustment, (d) the target electron distribution, and (e) electrons statistics in each irradiation area of vertical elliptical beam spots.

irradiation area, resulting in different radiation dose rates. It can be observed that adjusting this parameter effectively controls the irradiation profile on the target, which is particularly important when there is a requirement for fast switching of irradiation modes or providing different dose rates for studying mechanisms related to irradiation-induced material modifications.

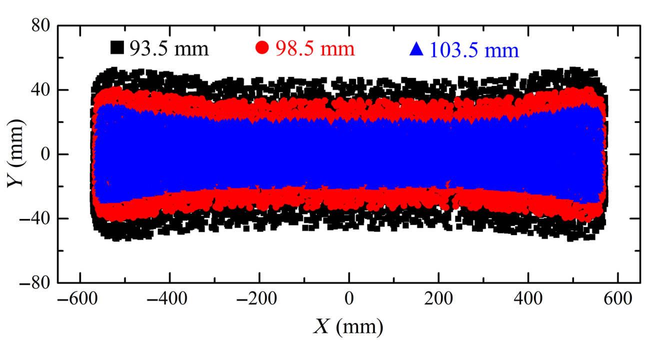

FIG. 19. Beam control effect of the coupled magnetic field of the doublet.

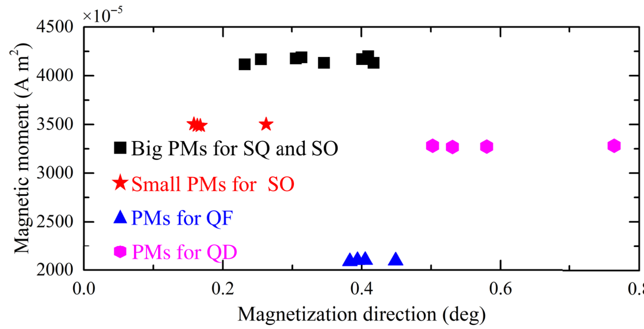

FIG. 20. The magnetic performance of each PM.

It should be noted that there exist numerous magnet control strategies for any given beam spot; however, determining an optimal control strategy depends on factors such as electron irradiation accelerator structure and irradiation environment conditions. Through flexible magnet adjustment, a uniform spreading beamline can provide good beam distribution and homogeneity for various spot shapes or irradiation conditions, demonstrating its broad applicability.

IV. MAGNETS FABRICATION

A. Permanent magnets

Magnetic errors refer to imperfections in the characteristics of PM, such as the fluctuations of magnetic moment and magnetization direction from the ideal value [43]. To measure the performance of each PM, a 3D composite Helmholtz coil is utilized. As shown in Fig. 20, the magnetization deflection angle is less than 1°, and the relative error of the magnetic moment does not exceed 1%, which helps reduce magnetic field errors and excessive shifts at the center of the magnetic field for all magnets.

B. Tunable yokes

The different adjustment strategies discussed in Sec. III are based on changes to the layout of PMs within the yoke; thus, ensuring tunable yokes serve as a foundation for this function. The fabricated yokes and magnets are displayed in Fig. 21. Rectangular PMs are embedded directly in the yoke as the magnetic poles. The PMQ doublet consists of two PMQs, which are connected by screws and nuts. Additionally, a magnet sleeve is used to hold the magnetic pole on the same side of the spreading system and is connected externally by a rotating nut and screw. This allows for flexible adjustment of the distance between magnets on the same side in the spread system to modify the magnetic field distribution. All yokes are made from soft iron (DT4) marked with scales for precise positioning.

C. Magnetic field measurement

The machining error for PMs is ±0.1 mm and for magnetic yokes, it is ±0.05 mm. Additionally, performance errors in PMs can also result in differences between

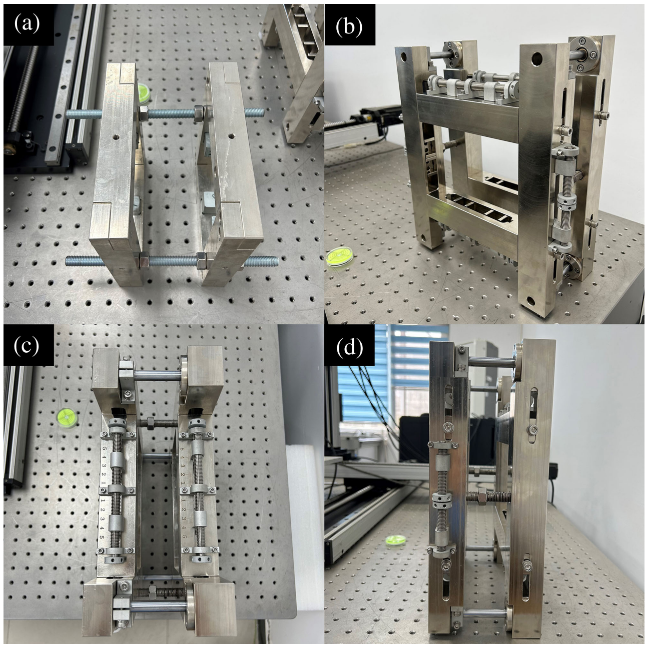

FIG. 21. Yokes of (a) PMQs doublet, (b) spreading system and its detail structure control screw of (c) big magnets (d) small magnets.

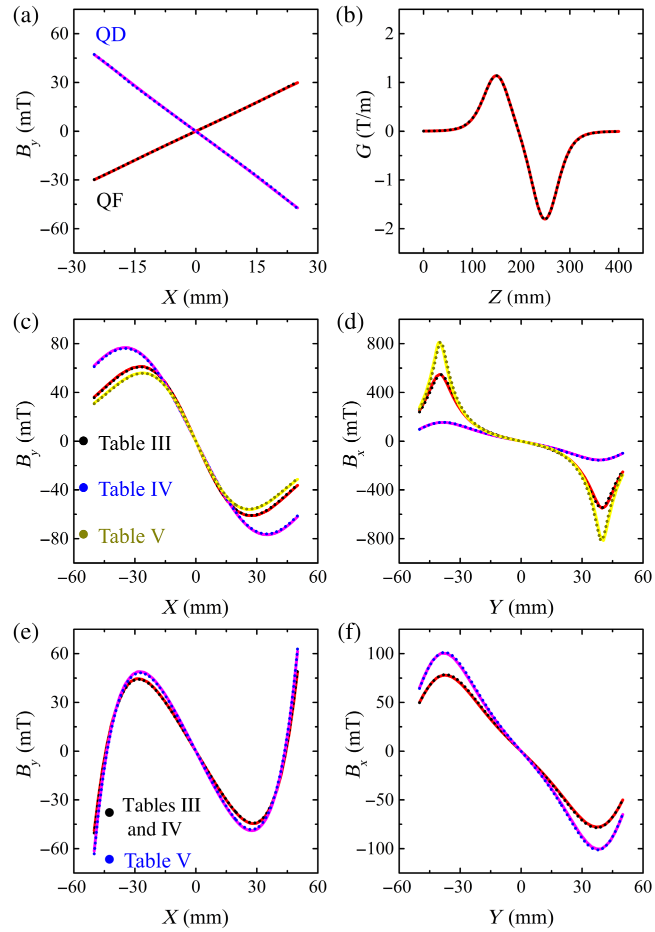

FIG. 22. Comparison between the measured magnetic field represented by the points and the simulated magnetic field represented by the solid lines: (a) QD and QF; (b) doublet; (c) B_y on horizontal direction and (d) B_x on vertical direction of SQ; (e) B_y on horizontal direction and (f) B_x on vertical direction of SO.

the actual and simulated magnetic field strengths. As a safeguard before applying magnets to an actual accelerator, magnetic field measurements are taken. For the PMQ doublet, the central magnetic field strength of two sets of PMQs and the magnetic field gradient of the doublet are measured. For SQ and SO, which are special tunable magnets that can be adjusted, their magnetic field distribution is measured in three corresponding states as described in Sec. III. The final magnetic field measurement results are nearly consistent with simulation results as shown in Fig. 22, which benefits from the performance screening of PMs to reduce the error.

V. SUMMARY AND OUTLOOK

The uniform spreading beamline, consisting of a PMQ doublet and a spreading system with rectangular permanent magnets as magnetic poles, is well suited for the compact space design of the electron irradiation accelerator. Addressing the issue of poor irradiation homogeneity caused by irregular beam spots that traditional electron irradiation accelerators struggle to solve, this beamline improves the irradiation homogeneity of circular and elliptical beam spots to over 91% while ensuring target irradiation shape, and even over 95% inside the target. Additionally, it allows for fast switching between different modes of irradiation on the target and adjustment of radiation dose rate according to scientific research or production processing requirements. The yoke structure maximizes flexibility in magnet configuration. Permanent magnet screening and magnetic field measurement results ensure engineering feasibility with an error between measured and simulated magnetic fields being less than 1%. In future applications to actual electron irradiation accelerators, this beamline will provide novel solutions for upgrading the irradiation processing industry.

ACKNOWLEDGMENTS

This work was supported by the National Natural Science Foundation of China (Grant No. 11975106) and the Program for HUST Academic Frontier Youth Team (2019QYTD06).

[1] O. N. Tretinnikov, S. Ogata, and Y. Ikada, Surface crosslinking of polyethylene by electron beam irradiation in air, Polymer **39**, 6115 (1998).

[2] J. Y. Lee, Y. M. Lee, B. Bhattacharya, Y. C. Nho, and J. K. Park, Separator grafted with siloxane by electron beam

irradiation for lithium secondary batteries, Electrochim. Acta **54**, 4312 (2009).

[3] K. Sheng *et al.*, Electron beam in-situ ultrafast curing of loadable primer-free polydimethylsiloxane coatings for composite insulators, Appl. Surf. Sci. **621**, 156830 (2023).

[4] H. Minamimoto, H. Irie, T. Uematsu, T. Tsuda, A. Imanishi, S. Seki, and S. Kuwabata, Polymerization of room-temperature ionic liquid monomers by electron beam irradiation with the aim of fabricating three-dimensional micropolymer/nanopolymer structures, Langmuir **31**, 4281 (2015).

[5] R. C. Dhuley *et al.*, Design of a 10 MeV, 1000 KW average power electron-beam accelerator for wastewater treatment applications, Phys. Rev. Accel. Beams **25**, 041601 (2022).

[6] M. N. Martins and T. F. Silva, Electron accelerators: History, applications, and perspectives, Radiat. Phys. Chem. **95**, 78 (2014).

[7] Z. Zimek, Impact of electron accelerator technical and economic parameters on unit cost of radiation processing, Radiat. Phys. Chem. **189**, 109713 (2021).

[8] Q. Wei, J. Mei, and J. Xie, Application of electron beam irradiation as a non-thermal technology in seafood preservation, LWT **169**, 113994 (2022).

[9] D. N. Nguyen *et al.*, Degradation of tricyclazole from aqueous solution and real wastewater by electron-beam irradiation, Environ. Technol. Innov. **21**, 101315 (2021).

[10] C. Tosri, K. Chusreeaeom, M. Limtiyayotin, N. Sukin, and P. Jompuk, Comparative effect of high energy electron beam and 137Cs gamma ray on survival, growth and chlorophyll content in Curcuma hybrid "Laddawan" and determine proper dose for mutations breeding, Emir. J. Food Agric. **31**, 321 (2019).

[11] B. Bita, E. Stancu, D. Stroe, M. Dumitrache, S. C. Ciobanu, S. L. Iconaru, D. Predoi, and A. Groza, The effects of electron beam irradiation on the morphological and physicochemical properties of magnesium-doped hydroxyapatite/chitosan composite coatings, Polymers (Basel) **14**, 582 (2022).

[12] S. Y. Kim, H. E. Gang, G. T. Park, H. Bin Jeon, H. Bin Kim, S. H. Oh, and Y. G. Jeong, Synergistic effect of polyurethane-coated carbon fiber and electron beam irradiation on the thermal/mechanical properties and long-term durability of polyamide-based thermoplastic composites, Polym. Compos. **43**, 1685 (2022).

[13] K. Sheng, X. Dong, Z. Chen, Z. Zhou, Y. Gu, and J. Huang, Increasing the surface hydrophobicity of silicone rubber by electron beam irradiation in the presence of a glycerol layer, Appl. Surf. Sci. **591**, 153097 (2022).

[14] K. Sheng, Y. Li, H. Li, Z. Ding, T. Chen, J. Yuan, C. Zuo, L. Zhang, P. Liu, and J. Huang, Electron beam irradiation enhanced varistor properties in ZnO nanowire, Appl. Phys. Lett. **117**, 021903 (2020).

[15] P. F. Meads, A nonlinear lens system to smooth the intensity distribution of a Gaussian beam, IEEE Trans. Nucl. Sci. **30**, 2838 (1983).

[16] E. Kashy and B. Sherrill, A method for the uniform charged particle irradiation of large targets, Nucl. Instrum. Methods Phys. Res., Sect. B **26**, 610 (1987).

[17] B. Sherrill, J. Bailey, E. Kashy, and C. Leakeas, Use of multipole magnetic fields for making uniform irradiations, Nucl. Instrum. Methods Phys. Res., Sect. B **40–41**, 1004 (1989).

[18] B. Blind, Production of uniform and well-confined beams by nonlinear optics, Nucl. Instrum. Methods Phys. Res., Sect. B **56–57**, 1099 (1991).

[19] F. Meot and T. Aniel, Principles of the non-linear tuning of beam expanders, Nucl. Instrum. Methods Phys. Res., Sect. A **379**, 196 (1996).

[20] Y. Yuri, N. Miyawaki, T. Kamiya, W. Yokota, K. Arakawa, and M. Fukuda, Uniformization of the transverse beam profile by means of nonlinear focusing method, Phys. Rev. ST Accel. Beams **10**, 104001 (2007).

[21] A. S. Dhavale, V. Sharma, and A. Sharma, Development of scanning system for industrial accelerator, Rev. Sci. Instrum. **92**, 103302 (2021).

[22] B. Nayak and D. Bhattacharjee, Physics studies of a DC electron accelerator for industrial applications, J. Instrum. **15**, T01004 (2020).

[23] J. Sun, J. Long, S. He, H. Xu, and D. Feng, Manufacture of a continuous triangle-waveform scanning magnet power supply used in industrial irradiation acceleration, in *Proceedings of 2009 IEEE 6th International Power Electronics Motion Control Conference (IPEMC), Wuhan, China, 2009* (IEEE, New York, 2009), pp. 2551–2555, https://doi.org/10.1109/IPEMC.2009.5157834.

[24] L. K. Wah, M. Azhar, R. M. Chulan, S. A. Hashim, M. Mokhtar, Khaidawaton, H. Baijan, and R. M. Sabri, Development of the scanning power supply for 300 KeV electron accelerator, IOP Conf. Ser. **785**, 012037 (2020).

[25] P. G. Benny, S. A. Khader, and K. S. S. Sarma, A study on beam profile of an industrial electron accelerator, Radiat. Eff. Defects Solids **173**, 705 (2018).

[26] J. Huang, Y. Q. Xiong, D. Z. Chen, K. F. Liu, J. Yang, D. Li, T. Q. Yu, M. W. Fan, and B. Yang, A permanent magnet electron beam spread system used for a low energy electron irradiation accelerator, Chin. Phys. C **38**, 107008 (2014).

[27] Z. Zhou, T. Chen, K. Sheng, and J. Huang, Magnetic field measurements and experimental verification of 0.5-MeV permanent-magnet electron-beam-spread system, AIP Adv. **12**, 095008 (2022).

[28] Z. Zhou, K. Sheng, J. Zou, T. Chen, and J. Huang, Study of irregular electron beam correcting permanent-magnet-quadrupole doublet lens for irradiation accelerator, Rev. Sci. Instrum. **94**, 023301 (2023).

[29] Y. K. Batygin, Beam intensity redistribution in a nonlinear optics channel, Nucl. Instrum. Methods Phys. Res., Sect. B **79**, 770 (1993).

[30] G. Ha, K. J. Kim, J. G. Power, Y. Sun, and P. Piot, Bunch shaping in electron linear accelerators, Rev. Mod. Phys. **94**, 025006 (2022).

[31] S. D. Gu and W. Bin Liu, Uniform transverse beam profile with a new type of nonlinear magnet, Chin. Phys. C **41**, 067003 (2017).

[32] K. Halbach, Design of permanent multipole magnets with oriented rare earth cobalt material, Nucl. Instrum. Methods **169**, 1 (1980).

[33] G. Tosin, P. Palma Sanchez, J. F. Citadini, and C. Castro Vergasta, Super hybrid quadrupoles, Nucl. Instrum. Methods Phys. Res., Sect. A **674**, 67 (2012).

[34] A. Ghaith *et al.*, Tunable high gradient quadrupoles for a laser plasma acceleration based FEL, Nucl. Instrum. Methods Phys. Res., Sect. A **909**, 290 (2018).

[35] A. Ghaith, D. Oumbarek, C. Kitégi, M. Valléau, F. Marteau, and M.-E. Couprie, Permanent magnet-based quadrupoles for plasma acceleration sources, Instruments **3**, 27 (2019).

[36] M. J. Easton, H. Li, Y. Lu, J. Zhu, and P. D. Pfister, Permanent-magnet quadrupoles for an interdigital H-mode drift tube linear accelerator: Optimization code and adjustable magnet design, Phys. Rev. Accel. Beams **21**, 122401 (2018).

[37] F. Marteau *et al.*, Variable high gradient permanent magnet quadrupole (QUAPEVA), Appl. Phys. Lett. **111**, 253503 (2017).

[38] T. Mihara, Y. Iwashita, M. Kumada, and C. M. Spencer, Variable permanent magnet quadrupole, IEEE Trans. Appl. Supercond. **16**, 224 (2006).

[39] J. A. Clarke, N. A. Collomb, B. J. A. Shepherd, D. G. Stokes, A. Bartalesi, M. Modena, and M. Struik, Novel tunable permanent magnet quadrupoles for the CLIC drive beam, IEEE Trans. Appl. Supercond. **24**, 1 (2014).

[40] Z. Zhou, Z. Zhang, and J. Huang, Design and optimization of high-current beam and long-range electron gun for 1 MeV electron irradiation accelerator, in *Proceedings of 2022 IEEE 3rd China International Youth Conference on Electrical Engineering (CIYCEE), Wuhan, China* (IEEE. New York, 2022), pp. 1–6, https://doi.org/10.1109/CIYCEE55749.2022.9959069.

[41] F. Ziaie, H. Afarideh, S. M. Hadji-Saeid, and S. A. Durrani, Investigation of beam uniformity in industrial electron accelerator, Radiation Measurements **34**, 609 (2001).

[42] H. Dorschner, W. Jenschke, and K. Lunkwitz, Radiation field distributions of an industrial electron beam accelerator, Nucl. Instrum. Methods Phys. Res., Sect. B **161–163**, 1154 (2000).

[43] P. N'gotta, G. Le Bec, and J. Chavanne, Hybrid high gradient permanent magnet quadrupole, Phys. Rev. Accel. Beams **19**, 122401 (2016).